JOURNAL OF MATERIALS SCIENCE 28 (1993) 6403–6408

Influence of multi-dimensional oscillating combustion fronts on thermal profiles

M. G. LAKSHMIKANTHA, J. A. SEKHAR
International Center for Micropyretics and Department of Materials Science and Engineering, University of Cincinnati, Cincinnati, OH 45221, USA

A multi-dimensional numerical model for micropyretic/combustion synthesis was developed and then applied to a special configuration. The configuration was chosen to illustrate the differences between one-dimensional and two-dimensional combustion. The features of the model include the melting of each constituent of the reactants and the products, and considerations of porosity for both the reactants and the products. Application of this model to the oscillatory combustion synthesis of TiB_2 has been carried out, for the first time, to study two-dimensional- combustion-front movement. The model predicts higher hot-spot temperatures in a two-dimensional situation than those obtained in a one-dimensional experiment. Additionally, hot spots are noted to traverse along orthogonal directions. Some processing implications of such results are examined.

Nomenclature

AP°, AP	Finite-difference coefficients
B	Breadth of specimen (m)
C_{PUA}	Specific heat of reactant A at 300 K ($J kg^{-1} K^{-1}$)
C_{PUB}	Specific heat of reactant B at 300 K ($J kg^{-1} K^{-1}$)
C_P	Specific heat of reactants at higher temperatures ($J kg^{-1} K^{-1}$)
C_{PU}	Specific heat of unreacted Reactants A and B at 300 K($J kg^{-1} K^{-1}$)
E	Activation Energy ($J mol^{-1}$)
H	Enthalpy ($J kg^{-1}$)
K	Dimensionless thermal conductivity
K_U	Thermal conductivity of the reactants A, B at 300 K($W m^{-1} K^{-1}$)
K_0	Frequency factor (s^{-1})
ΔH_{SLA}	Latent heat release at the melting point of Reactant A ($J kg^{-1}$)

Superscripts

n	New time level
o	Old time level
m	Iteration number

K^*	Thermal conductivity of A, B and AB in the reaction zone ($W m K^{-1}$)
L	Length of specimen (m)
M	Melting parameter
Q	Heat of reaction ($J kg^{-1}$)
R	Universal gas constant ($J mol^{-1} K^{-1}$)
t	Time (s)
T	Temperature (K)
T_C	Combustion temperature (K)
T_0	Ambient temperature (K)
X, Y	Dimensionless co-ordinates
X^*, Y^*	Co-ordinates (m)
ρ	Density of reactants at 300 K ($kg m^{-3}$)
$\varnothing$	Dimensionless enthalpy
θ	Dimensionless temperature
τ	Dimensionless time
η	Dimensionless fraction of reacted product

Subscripts

n	Northern side of control volume
N	Northern control volume
P	Centre of current control volume
s	Southern side of control volume
S	Southern control volume

1. Introduction

The recent interest in the development of new materials through combustion/micropyretic synthesis (CS) has brought into focus the importance of the various processing variables involved in this synthesis [1–4]. These processing variables are the reactant size, the compact pressure, the heating rate, the cooling rate and the initial temperature of the specimen; in combination they affect the final microstructure. Of these variables, those which affect the nature of the combustion front are the heat of reaction, the activation energy, the pre-exponential factor, the thermal conductivity and the density. Due to the large number of variables involved in micropyretic synthesis, a proper control of the processing of the micropyretic synthesized products is of importance.

Several papers [5–19] have dealt with the modelling of combustion synthesis using a one-dimensional analysis. There have also been numerous observations of oscillatory, spinning and other time-dependent modes of combustion [6–8]. Most of these studies are analytical in nature and have been obtained under

0022–2461 © *1993 Chapman & Hall*

conditions of steady-state combustion. The stability limit for the propagation of a pulsating exothermic reaction front in the condensed phase was established by Shkadinskii *et al.* [8] who showed that the boundary between stable and oscillatory combustion can be described by the following function:

$$\alpha = \frac{RT_c}{E}\left[9.1\frac{C_pT_c}{Q} - 2.5\right]$$

(see the nomenclature). Oscillating combustion takes place for $\alpha < 1$ and steady-state combustion may be obtained for $\alpha > 1$. Experimental verification of this numerically derived equation has been given in [6]. Oscillatory combustion results in an alternating increase and decrease of the temperature and velocity, and the front propagates in a succession of rapid and slow jumps resulting in a banded structure. A banded structure obtained after combustion may contain different phases in each band. Many of the analytical or numerical studies that have been reported to date have neglected porosity and phase-change effects. Recently Margolis *et al.* [9] included the effects of phase changes on the stability of the combustion front and derived an equation for the bifurcation of stable and unstable conditions of the combustion front. The bifurcation parameter was given by

$$\alpha = \frac{EQ}{2RC_pT_c^2(1-M)}$$

where M is the melting parameter $0 < M < 1$ [9]. In previous papers, an attempt was made to relate the microstructure to the macrosopic heat flow [10] and to the banding observed in CS microstructures [11].

The aim of the present paper is to illustrate the nature of the combustion obtained after ignition along two orthogonal directions. The problem was chosen to illustrate the difference between one-dimensional and multi-dimensional combustion fronts. Multi-dimensional analysis is required in the consideration of such a problem. Hence, a two-dimensional numerical model was used for the analysis of this problem. The model considers the phase change of all the reactants and products. The thermophysical and chemical variables are assumed to be constant in each state but are different in different zones of the solid, in the liquid and in the melting zone.

2. Formulation for combustion synthesis

2.1. Equations and non-dimensionalization

The energy equation for transient heat conduction in two dimensions, which includes a source term containing heat release due to a reaction is given by

$$\rho\frac{\partial H}{\partial t} = \frac{\partial\left(K^*\dfrac{\partial T}{\partial X^*}\right)}{\partial X^*} + \frac{\partial\left(K^*\dfrac{\partial T}{\partial Y^*}\right)}{\partial Y^*} + \rho QK_0(1-\eta)\exp(-E/RT) \quad (1)$$

Now define the following dimensionless parameters

$$\theta = \frac{C_{PU}(T-T_0)}{\Delta H_{SLA}}, \quad \varnothing = \frac{H}{\Delta H_{SLA}}$$

$$K = \frac{K^*}{K_U}, \quad X = \frac{X^*}{L}, \quad Y = \frac{Y^*}{B}, \quad \tau = K_0t \quad (2)$$

Using the above dimensionless parameters, Equation 1 may be recast as

$$\frac{\partial\varnothing}{\partial\tau} = \gamma_x\frac{\partial(K\partial\theta/\partial X)}{\partial X} + \gamma_y\frac{\partial(K\partial\theta/\partial Y)}{\partial Y} + (1-\eta)\nu\exp\left(\frac{-N}{1+\beta\theta}\right) \quad (3)$$

where

$$\gamma_x = \frac{K_U}{\rho L^2C_{PU}K_0}, \quad \gamma_y = \frac{K_U}{\rho B^2C_{PU}K_0}, \quad \nu = \frac{Q}{\Delta H_{SLA}}, \quad N = \frac{E}{RT_0}, \quad \beta = \frac{\Delta H_{SLA}}{C_{PU}T_0} \quad (4)$$

The above equation is solved simultaneously with the following mass-balance equation (a first-order reaction).

$$\frac{\partial\eta}{\partial\tau} = (1-\eta)\exp\left(\frac{-N}{1+\beta\theta}\right) \quad (5)$$

A detailed description of the variation of the thermophysical and chemical properties (such as the heat capacity, the thermal conductivity and the density of various reactants, like A and B and the product AB, are given in our earlier paper [11]. The porosity and phase-change effects are also described in that paper.

2.2. Finite-difference equations

The differential equation above, Equation 3, may be written in the finite-difference form as

$$(AP^\circ\varnothing_P^n + \theta_P^nAP - \text{RHS}) = \nu(1-\eta)\exp\left(\frac{-N}{1+\beta\theta_P^n}\right) \quad (6)$$

where the right-hand side (RHS) is given by

$$\text{RHS} = d_N\theta_N^n + d_S\theta_S^n + d_E\theta_E^n + d_W\theta_W^n + AP^\circ\varnothing^\circ$$

and

$$d_S = \frac{K_s\gamma_x}{(X_n - X_s)(X_P - X_S)},$$

$$d_N = \frac{K_n\gamma_x}{(X_n - X_s)(X_N - X_P)}$$

$$d_E = \frac{K_e\gamma_y}{(Y_w - Y_e)(Y_P - Y_E)},$$

$$d_W = \frac{K_w\gamma_y}{(Y_w - Y_e)(Y_W - Y_P)}$$

$$AP = d_N + d_S + d_W + d_E$$

$$AP^\circ = \frac{1}{d\tau} \quad (7)$$

X_n, X_s, X_N, X_S, X_P and Y's are shown in Figure 1, N refers to North, S to South, E to East and W to West.

The finite-difference equations are solved by an alternate-direction implicit procedure along with the Gauss–Seidal iterative method. Once the solution at

TABLE I The thermophysical/chemical constants used for TiB_2 in the calculations

Thermophysical constant	Reactants		Product TiB_2
	Ti	B (amorphous)	
Specific heats at 300 K, C_{PU} ($J\,kg^{-1}\,K^{-1}$)	528 [12]	118 [12]	950 [12]
Specific heats at higher temperatures, C_P	682 [12]	2455 [12]	1611 [12]
Specific heats in the liquid state C_{PL}	700 [12]	2800 [12]	2055 [12]
Thermal conductivities at 300 K K_U^* ($W\,m^{-1}\,k^{-1}$)	21.6 [12]	27	25 [12]
Thermal conductivities at higher temperatures K^*	13 [12]	18.4	16.8
Thermal conductivities in the liquid state, K^*_L	11 [12]	15	13
Densities at 300 K, ρ_u ($kg\,m^{-3}$)	4500 [12]	2450 [12]	4400 [12]
Densities at higher temperatures ρ ($kg\,m^{-3}$)	4300	2200	4200
Densities in the liquid state, ρ_L ($kg\,m^{-3}$)	4110 [12]	2080 [12]	4100
Melting points (K)	1933 [12]	2573 [12]	3190 [12]
Latent heats ($J\,kg^{-1}$)	0.175×10^5 [12]	0.193×10^5 [12]	0.185×10^5 [12]

TABLE II The values of various parameters used in the numerical calculations

Parameters	TiB_2
Activation energy, E	3.18×10^5 [13]
Heat of reaction, Q	4.214×10^6 [14]
Pre-exponential factor, K_0	1.5×10^{10}
Time step used, Δt	5×10^{-4}
Specimen size	$0.001 \times 0.001\ m^2$
Grid size	100×100

the old time level (o) is obtained, the initial solution of the new time level (n) is set equal to that of the old time level, and transient iteration begins.

3. Numerical procedure

The alternate-direction implicit scheme coupled with the Guass-Seidel iteration procedure is used for solving the equations. First, the temperatures and enthalpies at all nodes are initialized using the proper initial and boundary conditions. The number of nodes taken for the calculation was 101 per millimeter of the sample length for all the solutions. The grid size was 100×100. The time step used in the problem was 5×10^{-4} s. The information from the boundaries was carried into the interior of the specimen by first sweeping along the X-direction for half the time interval and then sweeping along the Y-direction for the other half of the time interval. At a given time, the reacted fraction of the current iteration was found using the values of the reacted fraction and the enthalpy of the earlier iteration. Using this value of the reacted fraction, the values of the heat capacity, the thermal conductivity and the density were calculated. Depending on the value of the reacted fraction and the enthalpies, equations in the appropriate zones were used for the calculations. The convergence criteria used to ascertain whether the reacted fraction at each time level had converged or not were obtained from the relative-error criterion, that is, from $|\eta^{m+1} - \eta^m/\eta^m|$ for all nodes $\leqslant \varepsilon$. The value of ε used was 1×10^{-6}. In each zone, the exponential source term was calculated using the enthalpies of the earlier iteration. In the appropriate zone, at a given point, the enthalpy was calculated for the current iteration. The convergence

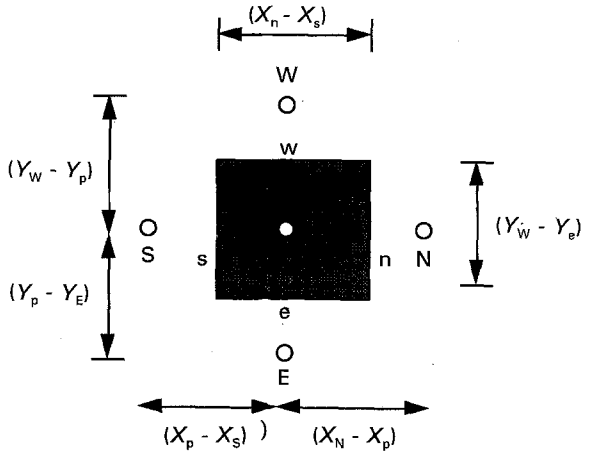

Figure 1 Sketch showing the co-ordinates in the N–S and E–W directions.

criteria used to ascertain whether the solution at each time level had converged or not was obtained from the relative-error criterion, that is, from $|\varnothing^{m+1} - \varnothing^m/\varnothing^m|$ for all nodes $\leqslant \varepsilon$. The value of ε used for checking convergence was 0.001. Once the convergence was reached, the enthalpy of the last iteration in a time step was considered as the final value of the enthalpy at that point. The calculations were performed for various times depending upon the problem.

4. Results and discussion

The solutions corresponding to the combustion synthesis of TiB_2 are presented. The reactants were Ti and B in stoichiometric composition of TiB_2. The liquidus for this composition is 3190 K [12]. The densities, thermal conductivities and heat capacities are assumed to be independent of temperature but they are different in each state. The average values of these thermophysical values varies as the reaction proceeds depending upon the degree of reaction. Table I gives the values of the thermophysical/chemical values for the reactants, Ti and B, and the product TiB_2. Table II gives the values of various other parameters used in the numerical analysis.

The first numerical experiment involved a square preform of material (TiB_2) ignited along only one

edge. The temperature along the ignited edge was taken to be 3190 K, which is the adiabatic combustion temperature of TiB_2. Adiabatic conditions were assumed on the three other edges. Fig. 2a shows the two-dimensional configuration and other boundary conditions chosen in the first numerical experiment. Fig. 3 shows the nature of the thermal profile at a dimensionless time of 0.585×10^8. The other conditions used were equal values of porosity (50% porosity) for both reactants and product. As may be noted from

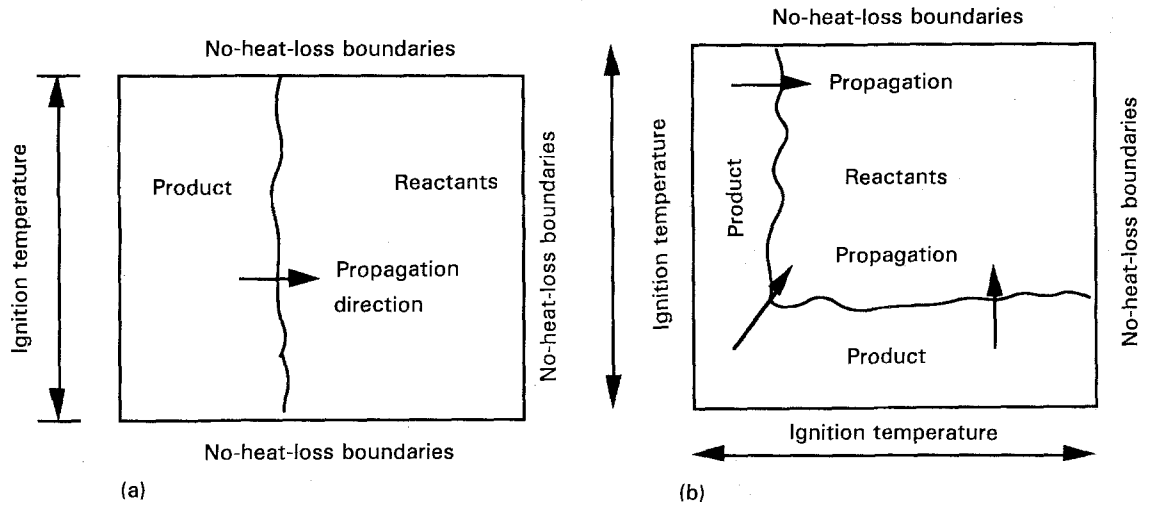

Figure 2 Schematics of the two-dimensional configuration and the various boundary conditions chosen in (a) the first and (b) the second numerical experiment.

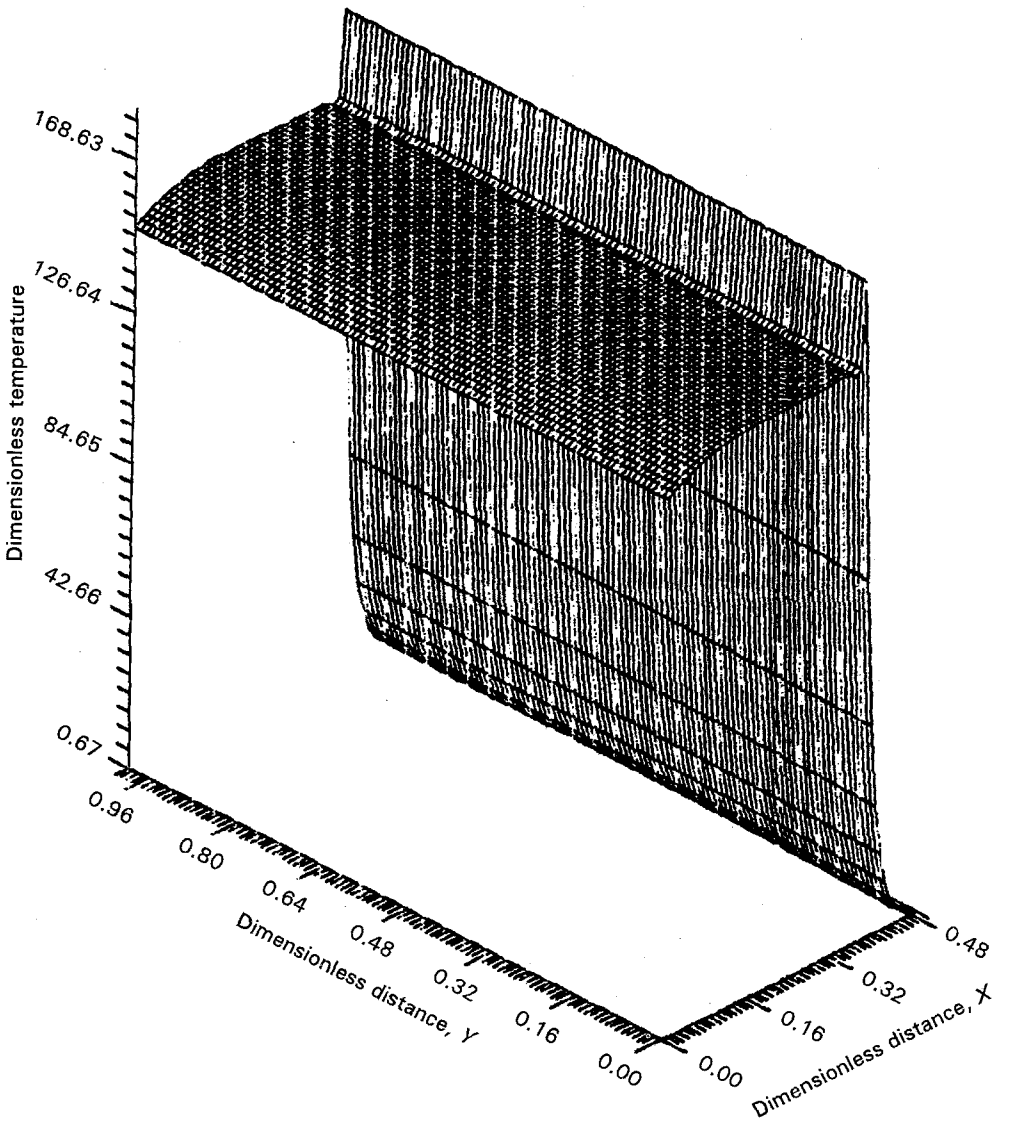

Figure 3 A three dimensional plot of the dimensionless-temperature profile at a dimensionless time of 0.585×10^8 along the length of the specimen.

Fig. 3, the nature of thermal profile is oscillatory (that is, the temperature of the combustion front is higher than the adiabatic temperature).The thermal gradient is only in the X-direction. Oscillations only occur in this direction. It should be further noted that the velocity and temperature profile obtained are similar to those obtained from previous one-dimensional numerical experiments [11]. The average velocity of propagation obtained in the X-direction was $0.117\ m\ s^{-1}$. The hot spot, or the peak dimensionless temperature, was 182.5 (note, in comparison, that the dimensionless adiabatic combustion temperature was 152).

The second numerical experiment considered igniting the square sample on the two adjacent sides along the X- and Y-directions with adiabatic conditions on

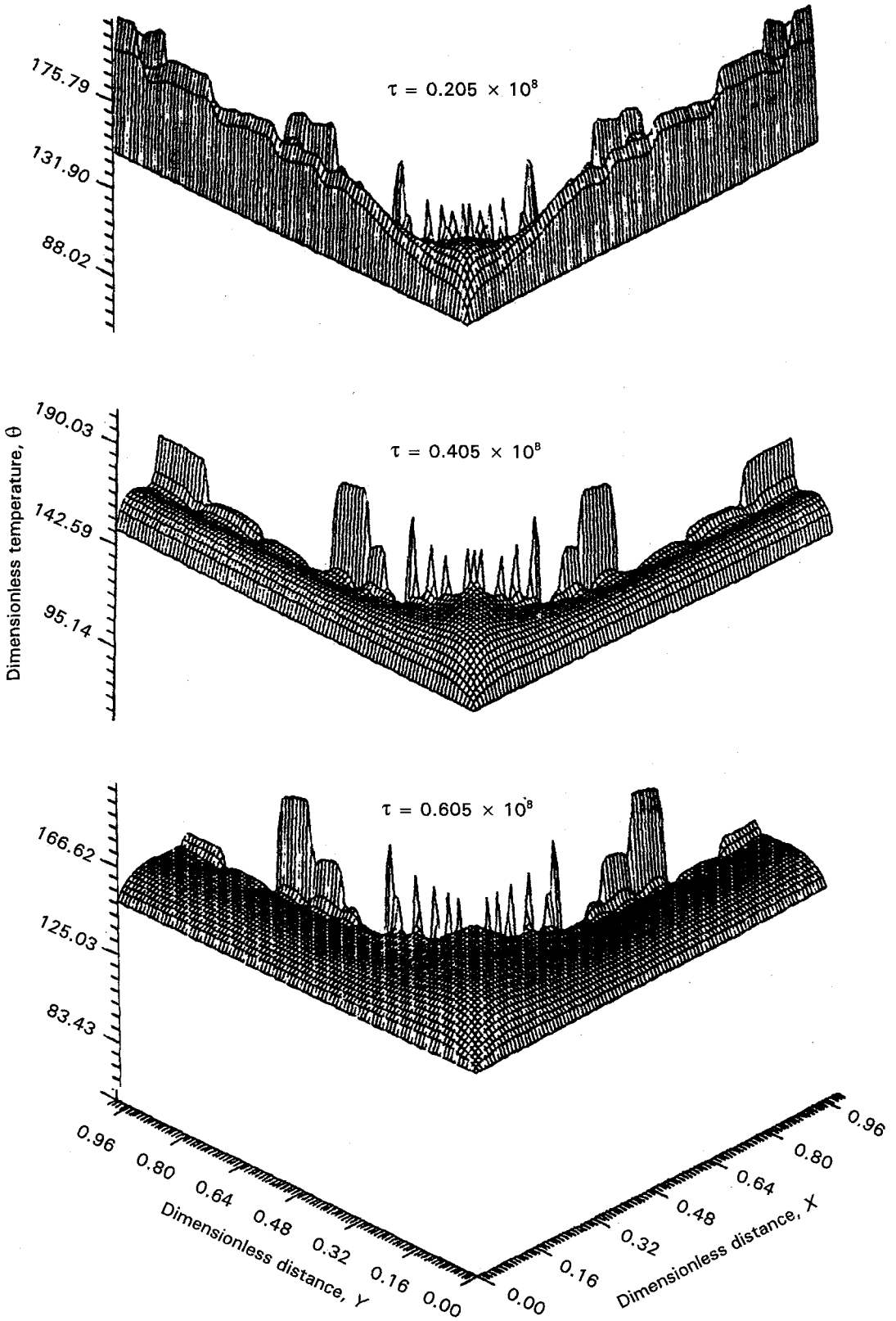

Figure 4 A three-dimensional plot of the dimensionless-temperature profiles at dimensionless times of: (a) 0.205×10^8, (b) 0.405×10^8, and (c) 0.605×10^8.

the remaining two sides. The ignition temperature corresponded to an adiabatic dimensionless temperature of 152. Fig. 2b shows the two-dimensional configuration and other boundary conditions chosen in the second numerical experiment. Fig. 4 shows the thermal profiles at dimensionless times of 0.205×10^8, 0.405×10^8 and 0.605×10^8, respectively. The first observation that may be noted is that the hot-spot temperature was 205.5; this is considerably higher than 182.5 which was obtained in the earlier experiment. The reason for this increase in the hot-spot temperatures is that particles of unreacted reactants in the reaction zone experience thermal gradients in both the X- and Y-directions thus leading to the higher hot-spot temperature. The second observation that may be noted from Fig. 4b and c is that there are specific regions of hot-spot temperatures along both the X- and Y-directions. It should be noted that the maximum temperatures near the wave front along the Y-axis at a given X-axis position are not equal. This results in a high thermal gradient along both the X- and Y-axes. Comparing the positions of the hot-spot regions in Fig. 4b and c, it may be noted that the hot-spot regions move along both the X- and Y-directions as time increases. Since the maximum temperatures near the combustion front along the Y-axis at a given X-value are not equal, the instantaneous and average cooling rates (or solidification rate) after the combustion would not be the same along this line. Hence staggered striations on the surface of the sample may be expected. Such banded structures in both the longitudinal and transverse directions have been observed in experiments [15]. Further, the hot-spot temperatures are also different in the one- and two-dimensional situations. Hence it is expected that microstructures with different properties will be noted in the above two experiments. The processing implications of this can be significant. For example, an experiment performed in a furnace with an atmosphere at a higher initial temperature produces microstructures which depend on the position and the direction of ignition of the sample. Due to local inhomogenities in the sample, and also because of the sensitiveness of the combustion, the sample in the furnace may be ignited at one or more points of the sample, thus leading to the two-dimensional instabilities discussed in this article. In addition, the microstructure development is influenced by the local temperatures developed during micropyretic synthesis. Clearly then, proper control of ignition during combustion synthesis is necessary in order to achieve uniform and reproducible properties in a combustion-synthesized product.

5. Conclusion

A multi-dimensional numerical model for micropyretic synthesis has been used in the analysis of TiB_2 formation. The model predicts higher hot-spot temperatures in a two-dimensional situation than in a one-dimensional experiment. Additionally, hot spots transverse along orthogonal directions.

Acknowledgements

The work was carried out as a part of Grant No. AFOSR-90-0308, monitored by Dr Alan Rosenstein. A grant by the Ohio Supercomputer Center, Grant No. PES441-2, for time on the CRAY Y-MP8/864 is also gratefully acknowledged.

References

1. J. B. HOLT and Z. A. MUNIR, *J. Mat. Sci.* **21** (1986) 251.
2. K. A. PHILPOT, Z. A. MUNIR and J. B. HOLT, *ibid.* **22** (1987) 159.
3. H. P. LI, S. BHADURI, and J. A. SEKHAR, *Metall. Trans. A* **23** (1992) 251.
4. C. T. HO and J. A. SEKHAR, 'High temperature ordered intermetallic alloys', Materials Research Society, Pittsburgh, PA, (1991) 1057.
5. A. G. MERZHANOV and B. I. KHAIKIN, *Prog. Energy Combust. Sci.* **14** (1988) 1.
6. Y. S. NAIBORODENKO and V. I. ITIN, *Comb. Explos. Shock Wave* **11** (1975) 293.
7. J. PUSZYNSKI, J. DEGREVE and V. HLAVACEK, *Ind. Engng. Chem. Res.* **26** (1987) 1424.
8. K. G. SHKASHINSKII, B. I. KHAIKIN and A. G. MERZHANOV, *Comb. Explos. Shock Waves* **7** (1971) 15.
9. S. B. MARGOLIS, H. G. KAPER, G. I. LEAF and B. J. MATKOWSKY, *Combust. Sci. Technol.* **43** (1985) 127.
10. M. G. LAKSHMIKANTHA, A. BHATTACHARYA and J. A. SEKHAR, *Metall. Trans. A* **23** (1992) 23.
11. M. G. LAKSHMIKANTHA and J. A. SEKHAR, *ibid.* **24** (1993) 614.
12. E. A. BRANDES, "Smithells metals reference book", 6th Edn, (Butterworth, London, 1976).
13. "Materials hand book for refractories: traditional and advanced ceramics" (Ceramic Industry, McGraw-Hill, New York, in press, 1991).
14. G. V. SAMSONOV and I. M. VINITSKII, "Handbook of refractory compounds", (IFI/Plenum, New York, 1980) 128.
15. H. P. LI and J. A. SEKHAR, *J. Mater. Res.* **8**(10) (1993).

Received 4 February
and accepted 17 May 1993